Supporting Information

Cho et al. 10.1073/pnas.1017082108

SI Discussion

As noted in the main-text *Discussion*, there are epidemiological studies exploring the relationship between metformin and a variety of cancers, and metformin-treated patients appear to have decreases in some types of cancer (1, 2). However, metformin is administered to patients to treat type II diabetes, commonly in association with obesity. Accordingly, the biological effects and epidemiological findings reflect a complex interplay among numerous variables—some of which are cancer cell-intrinsic but many of them extrinsic to the tumor cells. For instance, obesity and type II diabetes are now appreciated as commonly involving inflammation that is exacerbated or reinforced by the results of insulin resistance (3–5). Inflammation in turn is understood to influence the emergence of cancers via the tumor microenvironment (6). Moreover, the concentrations of blood sugar, other metabolic substrates (e.g., fatty acids), and hormones and cytokines such as IGF1 all impact both the nascent tumor cell and the host. All of these factors are affected by treatment with hypoglycemic agents such as metformin. Accordingly, although it has been reported that treatment of diabetics with metformin decreases their relative risk for some types of cancer (with little or no information about lymphomas) (1, 2), these studies cannot sort out the complex interplay among these multiple variables and, in particular, what are tumor cell-intrinsic effects.

Survival, proliferation, and developmental regulation can affect the emergence and progression of B lymphoma and other cancers. Our experiments showed that for the B lymphocyte, PARP14 promotes metabolic fitness and a higher probability of survival and that metformin can normalize these parameters for PARP14-deficient B-lineage cells. A reasonable and exciting inference supported but not proven by these findings is that they may highlight a dualistic impact of metabolism or metformin (or AMPK activation) as a feature of the findings about cancer. The enhanced metabolic fitness might, at the tumor cell-autonomous level, increase cancer fitness while decreasing risks in the setting of the organism as a whole. Such "Jekyll and Hyde" behavior is now appreciated for TGF-β, for instance (7). Consistent with these points, evidence from metformin chemoprevention studies in a lung cancer model suggests that in this experimental setting, a protective influence of metformin is due not to its effects on the tumor cells themselves but rather to metformin's impact on the liver, that is, decreased production of circulating proteins such as IGF1 that enhance the cancer (1). This experimental evidence supports the important conceptual point that metformin systemically might attenuate cancers by indirect mechanisms, even though in the evolving cancer cell it might promote metabolic fitness.

SI Materials and Methods

Mice. Mice were housed in the Vanderbilt University mouse facility under Institutional Animal Care and Use Committee guidelines and used following approved protocols. With the exception of tumor incidence analyses, mice were used at 5–10 wk of age. For monitoring and scoring lymphoma incidence, Eμ-*myc* mice were maintained until scored as positive when compromised by disease with palpable tumor or clearly suffering or moribund, according to guidelines of the Institutional Animal Care and Use Committee and veterinary staff.

Reagents, Cell Purification, Cytokines, and Cell Culture. LY294002, metformin, and compound C were obtained from Calbiochem. Recombinant mouse IL-4 was purchased from BD Biosciences; IL-6, IL-3, and murine stem cell factor (SCF) were from Peprotech; and $F(ab')_2$ of goat anti-mouse IgM was from Jackson ImmunoResearch Laboratories. GFP-Glut-1 ligand ($H2_{RBD}$-EGFP) fusion protein (8, 9) was a generous gift of N. Taylor and M. Sitbon (Universite de Montpellier, Montpellier, France). Mouse primary lymphocytes were cultured as described (10). Depletion of $Thy1^+$ cells from the splenocyte pool was performed using biotin-anti-Thyl.2 and streptavidin magnetic beads (BD IMag; BD Biosciences).

Bone Marrow Reconstitutions. Bone marrow cells from femurs and tibiae of 8- to 10-wk-old mice were harvested and transduced after induction of donors with 5-fluorouracil (11). Transductions were performed using supernatants from ΦNX packaging cells 2 d after transfection with MiT vector or MiT-PARP14(MC) as described (10). After expansion in Dulbecco's MEM supplemented with 15% FBS, 10 ng/mL IL-6, 6 ng/mL IL-3, and 100 ng/mL SCF, transduced cells (2×10^6 per recipient) were injected i.v. into irradiated (8 Gy in two divided doses) WT mice (8-wk-old). In parallel, controls (B6.PL-Thyla) received nontransduced marrow from WT and *Parp14*$^{-/-}$ mice. After 6 wk, $Thy1.1^+$ (transduced) and $Thy1.1^-$ B cells were isolated from the spleens of recipient mice using negative selection with anti-CD3ε magnetic beads followed by enrichment with biotinylated anti-Thyl.l for positive and negative selection. The enriched cell populations were then divided, cultured overnight ±IL-4, and assayed for apoptosis and glycolysis (modified by using 0.3 × 10 cells per sample for the triplicates).

Flow Cytometry and Apoptosis Assays. Antibodies were from BD Biosciences unless otherwise indicated. Cells were analyzed using flow cytometry with a FACSCalibur (BD Biosciences) and FlowJo software (TreeStar) as described. TUNEL assays were performed as described (12), using cells cultured (20 h) with or without IL-4 (5 ng/mL). Protection against apoptosis provided by IL-4 was quantitated using the formula ["% decrease in death" = (% $TUNEL^+_{medium\text{-}only}$ − % $TUNEL^+_{IL\text{-}4\text{-}treated}$)/(% $TUNEL^+_{medium\text{-}only}$)]. Surface levels of Glut-1 were measured using a translational fusion with GFP with a Glut-1 ligand ($H2_{RBD}$-EGFP) (8, 9). Cultured splenocytes were incubated with $H2_{RBD}$-EGFP at 37 °C for 30 min, surface-stained for B220, and analyzed by flow cytometry.

Measurements of RNA and Protein Levels. Proteins in whole-cell extracts were separated by SDS/PAGE, transferred onto nylon membranes (Millipore), and then incubated with rabbit antibodies against phospho (p)-Akt (S473), p-Akt (T308), p-FOXOl/3a, p-GSK3p, Akt (Cell Signaling Technologies), and goat anti-actin (Santa Cruz Biotechnology) Abs followed by the appropriate fluorophore-conjugated, species-specific secondary anti-Ig antibodies (Rockland Immunochemicals and LI-COR). Bands were visualized and quantitated as described (12). RNA was isolated using TRIzol reagent (Invitrogen). After cDNA synthesis by reverse transcription, expression of metabolic genes was analyzed by quantitative real-time RT-PCR run in triplicate using SYBR Green (Applied Biosystems) and compared with levels of 36B4 as a control and the primer pairs detailed in Table S1. Data are presented as values normalized to WT control and averaged over three independent experiments.

Glucose Uptake and Glycolysis Assays. B cells (10^6 cells per sample) were cultured in RPMI1640 medium for 20 h at 37 °C in 5% CO_2 in the presence or absence of IL-4. To quantitate glycolysis after

culture, cells were washed and pulsed with 10 μCi of 5-[^{3}H]glucose in 24-well plates (37 °C, 1 h). The reaction was stopped with 0.2 N HCl, and ^{3}HOH generated from [5-^{3}H]glucose (13.5 Ci/mmol; PerkinElmer) was captured by diffusion into a reservoir of H_2O in a tightly sealed scintillation vial. Diffused and undiffused ^{3}H were then measured by liquid scintillation counting. To measure glucose uptake, equal numbers of viable cells were then incubated (37 °C, 15 min) in glucose uptake buffer (8.1 mM Na_2HPO_4, 1.4 mM KH_2PO4, 2.6 mM KCl, 136 mM NaCl, 0.5 mM $MgCl_2$, 0.9 mM $CaCl_2$, pH 7.4) to deplete intracellular glucose stores. Triplicate samples (10^6 cells per sample) were incubated with 1 μCi of 2-[1,2-^{3}H]deoxyglucose (20.7 Ci/mmol; PerkinElmer) in glucose uptake buffer for 2 min at room temperature and immediately spun through a layer of bromododecane into 20% perchloric acid/8% sucrose to stop the reaction and separate cells from unincorporated 2-[^{3}H]deoxyglucose. Recovered cell pellets carefully separated from all supernatant were counted by liquid scintillation.

Measurement of Mitochondrial Parameters, Glucose Oxidation, Surface Glut-1 Level, and Lactate Production. Cultured splenocytes were stained with MitoTracker Green (Invitrogen) for 45 min, surface-stained for B220, and analyzed by FACS gated on viable lymphoid cells. For the measurement of mitochondrial membrane potential, splenocytes were stained with DiOC6(3) dye for 15 min, surface-stained for B220, and analyzed by FACS. Alternatively, purified B cells were cultured with or without added IL-4 (20 h at 37 °C) and recounted after culture. Viable cells were replated (4×10^5 cells/200 μL) and incubated (3 h at 37 °C) with 3-[4,5-dimethylthiazol-2-yl]-2,5-diphenyltetrazolium bromide (5 μg/mL), after which the medium was removed and dye converted by mitochondrial reductases was solubilized with 0.1 N HCl/isopropanol. Converted dye was measured by its absorbance at 570 nm minus background at 640 nm. Glucose oxidation was measured by $^{14}CO_2$ generation from [6-^{14}C]glucose. After culture in the presence or absence of IL-4 for 20 h at 37 °C, viable cells (5×10^6 cells/mL) were incubated in glucose-free RPMI1640 medium for 30 min, 0.5 μCi of [6-^{14}C]glucose (50 mCi/mmol; American Radiolabeled Chemicals) was added, and this placed in a rubber-stoppered 20-mL scintillation vial containing a center well with 5% KOH-soaked filter paper. Following incubation (37 °C, 3 h), radioactivity of trapped $^{14}CO_2$ in the filter paper was measured by liquid scintillation counter. Fatty acid oxidation rates were measured using [^{3}H]palmitate. Viable B cells (4×10^6) were washed and incubated with 400 μL RPMI1640 medium containing 2% (wt/vol) fatty acid-free BSA, 0.25 mM L-carnitine, and [^{3}H]palmitic acid (2 μCi) for 4 h. Excess [^{3}H]palmitic acid in the medium was removed by trichloroacetic acid precipitation twice. The supernatant was extracted with chloroform:methanol (2:1) twice and then counted for ^3H_2O production. For the measurement of lactate production, purified splenic B cells were cultured in the presence or absence of IL-4 or LPS, and the culture medium was assayed for lactate levels using lactate reagent (Trinity Biotech) according to the manufacturer's instructions.

In Vivo BrdU Assay. Filter-sterilized 5-bromo-2′-deoxyuridine (BrdU; 50 μg/g body weight) dissolved in PBS was injected i.p. into the mice (6-wk-old), from which bone marrow cells were harvested 1.5 h later. After staining with anti-B220 and anti-IgM, cells were fixed with paraformaldehyde (4%), permeabilized with 0.2% saponin, 1% FBS in PBS, refixed (4% paraformaldehyde), treated (30 min at 37 °C) with 50 U DNase I (Roche), stained with Alexa647-anti-BrdU Ab (Invitrogen), and analyzed by flow cytometry.

Retroviral Transduction of AMPK Constructs. AMPK-CA (T172D mutant form) and AMPK-DN (a 312-aa truncation mutant) (13) were subcloned into the MiT retroviral vector. Purified splenic B cells were activated (20 h) with anti-IgM (1 μg/mL) and IL-4 (5 ng/mL), and transfected with retrovirus (MiT, MiT-AMPK-CA, or MiT-AMPK-DN). After 2 d, transduced (Thy1.1$^+$) and Thy1.1$^-$ B cells were isolated with biotinylated anti-Thy1.1 for positive and negative selection; the purified cell populations were then divided, cultured overnight ±IL-4, and assayed for apoptosis and glycolysis.

Quantitative Data and Statistics. Unless otherwise indicated, all bar graphs are presented as mean (±SEM) data from at least three independent biological replicate experiments, and * denotes $P < 0.05$ by appropriate significance testing.

1. Memmott RM, et al. (2010) Metformin prevents tobacco carcinogen–induced lung tumorigenesis. *Cancer Prev Res (Phila)* 3:1066–1076.
2. Jalving M, et al. (2010) Metformin: Taking away the candy for cancer? *EurJ Cancer* 46: 2369–2380.
3. Donath MY, Shoelson SE (2011) Type 2 diabetes as an inflammatory disease. *Nat Rev Immunol* 11:98–107.
4. Gregor MF, Hotamisligil GS (2011) Inflammatory mechanisms in obesity. *Annu Rev Immunol* 29:415–445.
5. Schenk S, Saberi M, Olefsky JM (2008) Insulin sensitivity: Modulation by nutrients and inflammation. *J Clin Invest* 118:2992–3002.
6. Mantovani A, Allavena P, Sica A, Balkwill F (2008) Cancer-related inflammation. *Nature* 454:436–444.
7. Bierie B, Moses HL (2006) Tumour microenvironment: TGFβ: The molecular Jekyll and Hyde of cancer. *Nat Rev Cancer* 6:506–520.
8. Manel N, et al. (2003) The ubiquitous glucose transporter GLUT-1 is a receptor for HTLV. *Cell* 115:449–459.
9. Kinet S, et al. (2007) Isolated receptor binding domains of HTLV-1 and HTLV-2 envelopes bind Glut-1 on activated CD4$^+$ and CD8$^+$ T cells. *Retrovirology* 4:31.
10. Goenka S, Boothby M (2006) Selective potentiation of Stat-dependent gene expression by collaborator of Stat6 (CoaSt6), a transcriptional cofactor. *Proc Natl Acad Sci USA* 103:4210–4215.
11. Otsu M, et al. (2002) Reconstitution of lymphoid development and function in ZAP-70-deficient mice following gene transfer into bone marrow cells. *Blood* 100: 1248–1256.
12. Cho SH, et al. (2009) PARP-14, a member of the B aggressive lymphoma family, transduces survival signals in primary B cells. *Blood* 113:2416–2425.
13. Stein SC, Woods A, Jones NA, Davison MD, Carling D (2000) The regulation of AMP-activated protein kinase by phosphorylation. *Biochem J* 345:437–443.

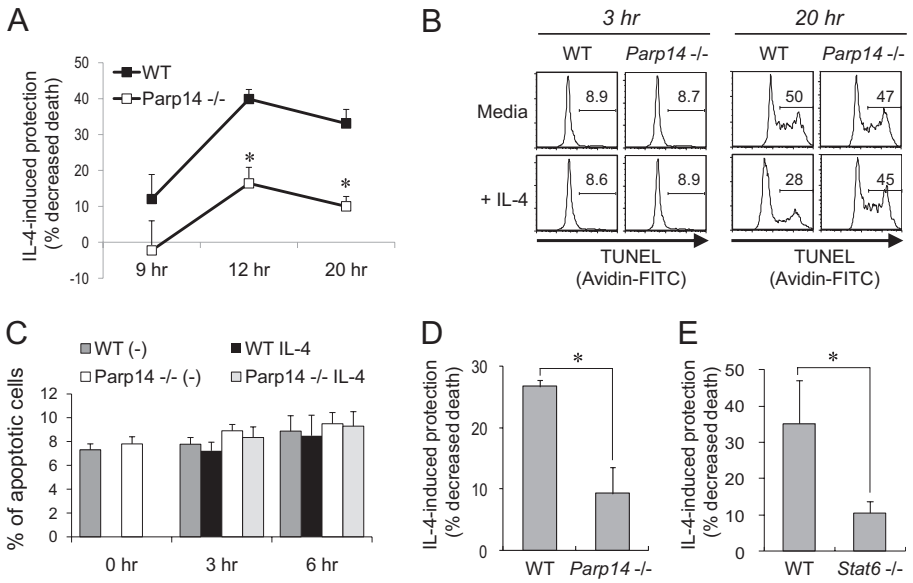

Fig. S1. Prosurvival effect of IL-4 depends on Stat6 and PARP14. (*A*–*C*) Splenocytes (WT and Parp14$^{-/-}$) were cultured with and without IL-4 for 3, 6, 9, 12, and 20 h, processed for TUNEL analysis, and scored by flow cytometry with gating on B220^{+} events. (*A* and *B*) PARP14 mediates IL-4–induced suppression of B-cell apoptosis starting after 9 h under culture conditions. (*A*) Shown are the mean (±SEM) results of three independent replicate time-course analyses of IL-4–induced protection against apoptosis. (*B*) Representative FACS profiles with TUNEL results from the B220^{+} gate in one of the experiments. (*C*) B cells remain viable past 6 h in culture. Shown are the mean (±SEM) TUNEL results with freshly isolated cells (to define the background signal of the flow cytometric TUNEL assay; "0 hr," hence no IL-4 treatment) and those cultured 3 or 6 h in the presence or absence of IL-4. (*D* and *E*) Shown are bar graphs plotting the aggregate results (mean ± SEM) of assays quantitating the suppression of apoptosis measured in TUNEL assays, of which representative results are shown in Fig. 1 *A* and *B*. B cells lacking PARP14 (*D*) or STAT6 (*E*) were cultured 20 h in the presence or absence of IL-4 in parallel with WT controls. The magnitude of protective effect provided by IL-4 was calculated as described in *SI Materials and Methods*.

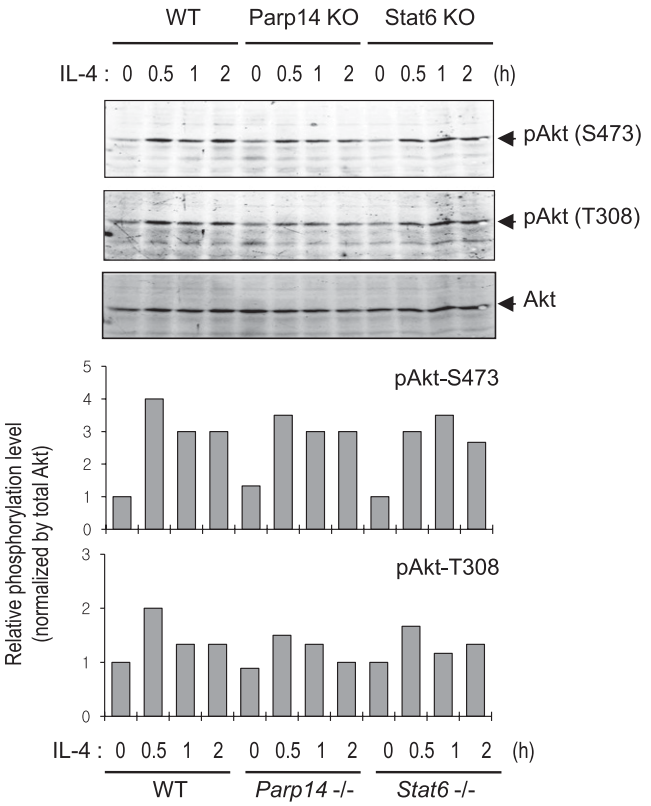

Fig. S2. Normal IL-4–induced phosphorylation of Akt in *Parp14*$^{-/-}$ and *Stat6*$^{-/-}$ B cells. B cells purified from WT, *Parp14* KO, and *Stat6* KO mice were stimulated with IL-4 for 30, 60, or 120 min or cultured without IL-4. Proteins in whole-cell extracts were analyzed by immunoblots using anti-pAkt (S473 or T308) and anti-Akt. Shown is an immunoblot result from one replicate experiment, with bar graphs quantitating the relative signal at each time point, normalized to the level of total Akt in the sample.

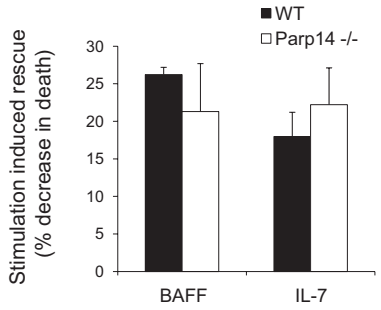

Fig. S3. PARP14 independence of survival signaling by BAFF and IL-7. WT and *Parp14*$^{-/-}$ splenocytes were cultured 20 h in the presence or absence of BAFF (10 ng/mL) or IL-7 (10 ng/mL), processed for TUNEL analyses, and scored by flow cytometry with gating on B220^{+} events. The magnitude of protective effect provided by BAFF or IL-7 was calculated as described in *SI Materials and Methods*.

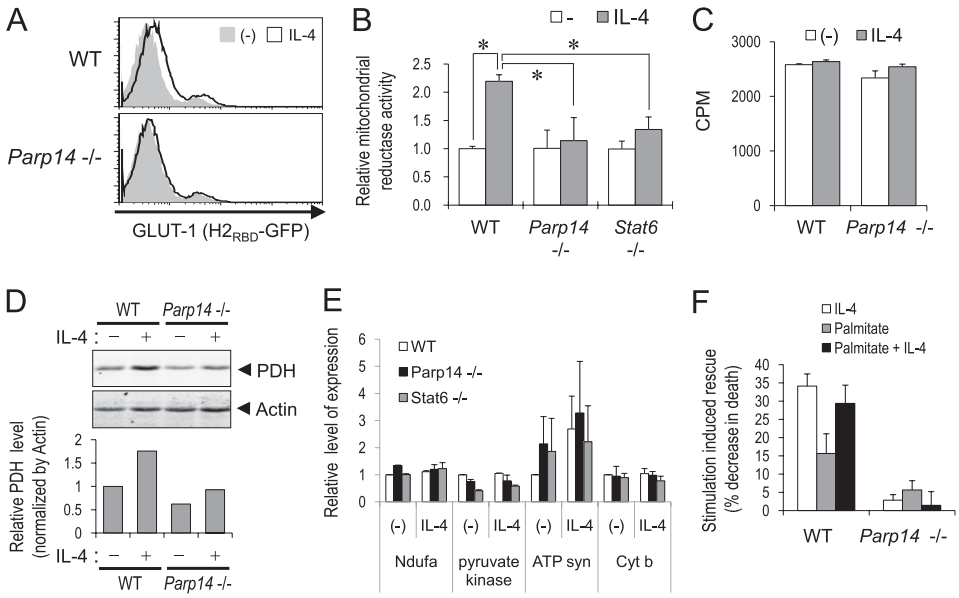

Fig. S4. PARP14 mediates IL-4–induced changes in metabolic activities in B cells. (*A*) PARP14 dependence on increased surface expression of Glut-1 hexose transport channel. WT and PARP14-null splenocytes were cultured in the presence or absence of IL-4 for 20 h. The surface level of Glut-1 was measured by Glut-1 ligand ($H2_{RBD}$-GFP) as described in *SI Materials and Methods*. Shown are the GFP profiles from the B220^{+} gate after flow cytometry of B cells stained with $H2_{RBD}$ after culture in the presence (open histograms) or absence (gray shaded histograms) of IL-4. (*B*) Mitochondrial reduction of a chromogenic substrate was measured in B cells purified from spleens of WT and *Parp14*$^{-/-}$ mice. Bar graphs represent the mean (±SEM) relative reductase activities. (*C*) Normal fatty acid oxidation rate in *Parp14*$^{-/-}$ B cells. Purified B cells from WT and *Parp14*$^{-/-}$ mice were cultured in the presence or absence of IL-4 for 20 h. Fatty acid oxidation was then measured using [^{14}C]palmitic acid. (*D*) PARP14 impacts pyruvate dehydrogenase (PDH) gene expression in IL-4–treated B cells. Extracts of B cells purified from spleens of WT and *Parp14*$^{-/-}$ mice, cultured as described in *A*, were used for immunoblot analyses. Shown is the result of probing with antibodies specific for PDH and actin, as indicated; the bar graph represents quantitation of the PDH signal after normalization to the actin band intensity. (*E*) Effect of IL-4 on expression of several genes involved in mitochondrial biogenesis. After determination of the optimal time for measuring increases in WT B cells, RNA was isolated from B cells cultured for 4 h with and without IL-4, and levels of mRNAs encoding metabolic genes (Ndufa, NADH-ubiquinone oxidoreductase 1 α subcomplex; pyruvate kinase; ATP syn, ATP synthase; Cyt b, cytochrome *b*) were analyzed by quantitative real-time RT-PCR analyses of cDNAs made from these RNAs. Bar graphs show mean (±SEM) relative expression, as for Fig. 4*E*. (*F*) Supplemental fatty acid was not sufficient to reverse the defect of IL-4–induced survival signals in *Parp14*$^{-/-}$ B cells. This dramatic increase in uptake likely reflects both the increased conversion of hexose through glycolytic demand and IL-4 -induced increases in surface expression of transporters such as GLUT-1 that are PARP14-dependent (*A*). Splenocytes (WT and *Parp14*$^{-/-}$) were cultured with and without IL-4 (5 ng/mL) or palmitic acid (20 μM) for 20 h, processed for TUNEL analysis, and scored by flow cytometry with gating on B220^{+} events.

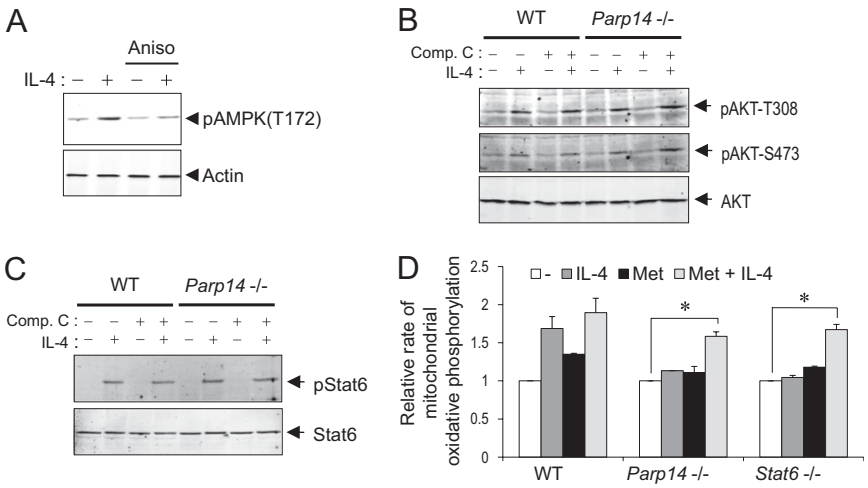

Fig. S5. AMPK function conditions the fitness of cells to respond to IL-4 by increased mitochondrial oxidation. (*A*) IL-4 activates AMPK in B cells by a protein synthesis-dependent mechanism. B cells purified from WT mice were cultured in the presence or absence of IL-4. Where indicated, cells were pretreated with the protein synthesis inhibitor anisomycin for 30 min before IL-4 stimulation. Extracts of purified B cells were analyzed by immunoblots using anti-phospho-AMPK(T172) Ab along with anti-actin as a loading control. Data shown are one representative result from three independent replicate experiments. (*B* and *C*) The AMPK inhibitor compound C did not interfere with IL-4–induced Akt (*B*) and Stat6 (*C*) phosphorylation. (*D*) Reversion of the defect of PARP14-deficient B cells in terms of IL-enhanced mitochondrial oxidative phosphorylation. After a 20-h culture in the presence or absence of IL-4 or metformin as indicated, mitochondrial oxidative phosphorylation was assayed in purified B cells as in Fig. 4*B*. Shown are mean (±SEM) data from three independent experiments (*$P < 0.05$).

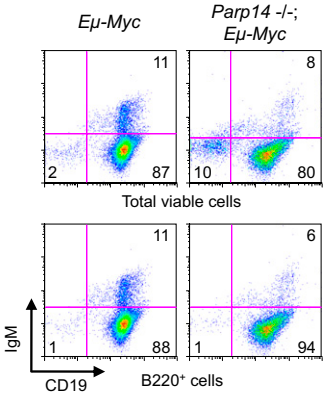

Fig. S6. Myc-induced PARP14-deficient lymphomas are of typical pre-B phenotype. Lymphoma tissue from four separate mice of each genotype was harvested at stages when the tumor nodules were palpable but of limited size, and single-cell suspensions were analyzed by flow cytometry. Shown are dot plots of CD19 versus IgM gated on total lymphocytes or the B220-positive gate, as indicated, from lymphomas in a representative *Parp14*-null and PARP14-sufficient mouse.

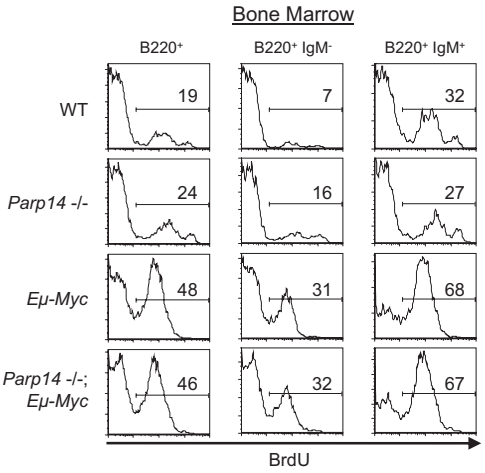

Fig. S7. Myc-driven proliferation of B-lineage progenitors in the prelymphomatous marrow is PARP14-independent. BrdU was injected into WT, *Parp14*$^{-/-}$, *Eμ-myc*, and *Eμ-myc*, *Parp14*$^{-/-}$ mice (age 6 wk) as described in *SI Materials and Methods*, after which bone marrow cells were surface-stained and processed to determine the fraction of the B-cell population that incorporated BrdU. Shown are FACS profiles of anti-BrdU signal gated on total B220^{+}, B220^{+} IgM^{-}, or B220^{+} IgM^{+} cells, as indicated.

Table S1. List of primer pairs used for key quantitative RT-PCR in Fig. 4

Primer name	Sequence
36B4 forward	5′-TCATCCAGCAGGTGTTTGAC-3′
36B4 reverse	5′-TACCCGATCTGCAGACACAC-3′
Glut-1 forward	5′-GCTGTGCTTATGGGCTTCTC-3′
Glut-1 reverse	5′-AGAGGCCACAAGTCTGCATT-3′
Citrate synthase forward	5′-TCTACTCACTGCAGCAACCC-3′
Citrate synthase reverse	5′-TGGCCTGCTCCTTAGGTATC-3′
Pyruvate dehydrogenase forward	5′-GTGTCCATGGTAGCGGTAAGTCT-3′
Pyruvate dehydrogenase reverse	5′-TTGCGGCTGCCTATTGC-3′
Succinate dehydrogenase forward	5′-AGAAGGCTGTGAAAAAATCAGTCA-3′
Succinate dehydrogenase reverse	5′-GGTCTGTGTTCCAAACCATTCC-3′

Table S2. Relative cell sizes by subset. Mean values for the forward scatter light signal in the flow cytometer were tabulated for the indicated subsets of B-lineage cells in bone marrow and spleen of mice of the indicated genotypes

	Bone marrow			Spleen	
	B220^{+}	B220^{+} IgM^{-}	B220^{+} IgM^{+}	B220^{+}	FOB
WT	347*	314	442	325	324
PARP14 KO	374	310	439	323	317
Eμ-*myc*	459	446	540	435	444
PARP14 KO/Eμ-*myc*	350	314	428	334	348

*Mean light intensity.